ARTICLE   OPEN

Check for updates

Stability improvement mechanism due to less charge accumulation in ternary polymer solar cells

Dong Xue[1], Masahiko Saito[2], Itaru Osaka[2] and Kazuhiro Marumoto [ID][1,3] ✉

Ternary polymer solar cells based on a thiazolothiazole-based polymer donor (PTzBT) and a fullerene acceptor (PC$_{61}$BM) have attracted attention because they show high efficiency and stability by addition of a non-fullerene acceptor (ITIC). However, the performance improvement mechanism is not completely elucidated. Here, we show the stability improvement mechanism due to less charge accumulation in the PTzBT cells with ITIC using operando electron spin resonance from a microscopic viewpoint. We observed two correlations between device performance and number of spins (N_{spin}) under solar irradiation. One correlation is the decrease in short-circuit current and the N_{spin} increase in electrons on PC$_{61}$BM and holes in PTzBT, where the ITIC addition causes the less these N_{spin}. The other correlation is the increase in open-circuit voltage and the N_{spin} decrease in holes in ZnO. These findings explain the stability improvement mechanism, showing the correlation between less charge accumulation and higher stability, which is valuable for the development of further efficient and stable polymer solar cells.

npj Flexible Electronics (2022)6:22 ; https://doi.org/10.1038/s41528-022-00153-z

INTRODUCTION

Polymer solar cells (PSCs) have been actively researched and developed as the next generation of solar cells due to their features such as flexibility, low production cost, and semitransparency, which are difficult to be achieved with silicon solar cells[1–3]. While binary blend systems in which a p-type material and an n-type material are mixed together to form a photoactive layer have been central to the PSCs, ternary blend systems have also been attracting much attention because they can effectively generate electricity by adding a p-type or an n-type third component material to the binary blend system, improving the power conversion efficiency (PCE)[4–8]. However, the performance improvement mechanism is still not completely elucidated from a microscopic viewpoint. Recently, it has been reported that the PCE of a binary blend PSC with a p-type semiconducting polymer based on poly((2,5-bis(3-(2-butyloctyl)thiophen-2-yl)thiazolo[5,4-d]thiazole)-alt-(2,5-bis(3-(2-hexyldecyl)thiophen-2-yl)thiazolo[5,4-d]thiazole)) (PTzBT) and an n-type semiconductor [6,6]-phenyl C$_{61}$ (or C$_{71}$)-butyric acid methyl ester (PC$_{61}$BM or PC$_{71}$BM) has markedly improved from 7.4% to 10.3% by adding a small amount of a narrow-band-gap non-fullerene acceptor 3,9-bis(2-methylene-(3-(1,1-dicyanomethylene)-indanone))-5,5,11,11-tetra-kis(4-hexylphenyl)-dithieno[2,3-d:2',3'-d']-s-indaceno[1,2-b:5,6-b'] dithiophene (ITIC) as a third component (Fig. 1a–c)[8]. Furthermore, the stability of the PTzBT cell has been enhanced by the ITIC addition, where the PCE decrease is reduced from 30% to 10% after storing the cells in a nitrogen-filled glove box for 1000 h at 85 °C under dark conditions[8]. As such the PTzBT ternary blend PSC is a promising cell with a high PCE and stability, ITIC is expected as a quite useful additive for improving the photovoltaic performance. Thus, it is interesting to elucidate the ITIC addition effect on the performance improvement mechanism of the PTzBT cells.

In previous electron spin resonance (ESR) studies on binary blend PSCs, clear correlations between device-performance deterioration and accumulated charges have been studied for typical binary blend PSCs with poly(3-hexylthiophene) (P3HT)[9], high PCE cells with poly[(4,8-bis-(2-ethylhexyloxy)-benzo(1,2-b:4,5-b)dithiophene)-2,6-diyl-alt-(4-(2-ethylhexyl)-3-fluorothieno[3,4-b] thiophene-)-2-carboxylate-2,6-diyl)] (PTB7)[10] and poly[4,8-bis(5-(2-ethylhexyl)thiophen-2-yl)benzo[1,2-b;4,5-b]dithiophene-2,6-diyl-alt-(4-(2-ethylhexyl)-3-fluorothieno[3,4-b]thiophene-)-2-carboxy-late-2,6-diyl)] (PTB7-Th)[11], and high stable cells with a copolymer based on poly[(2,5-bis(3-(2-butyloctyl)thiophen-2-yl)thiazolo[5,4-d] thiazole)-alt-(5,10-bis(4-(2-butyloctyl)thiophen-2-yl)naphtho[1,2-c:5,6-c']bis([1,2,5]thiadiazole) (PTzNTz)[12]. These reports have indicated that the accumulated charges contribute to the reduction of device performance. Although encapsulating the cells can eliminate the extrinsic degradation factors such as oxygen and moisture[13–15], the cell encapsulation cannot prevent charge accumulation[9–12]. The accumulated charge states in cells or materials can be directly observed and investigated by ESR spectroscopy at a molecular level[9–12,16–24]. It is very interesting to study the difference of accumulated charge states between binary and ternary blend PSCs and to clarify the effect of non-fullerene acceptor addition and the performance improvement mechanism of ternary blend PSCs.

Here, we performed operando light-induced ESR spectroscopy on the PTzBT:PC$_{61}$BM binary blend PSCs with and without ITIC to investigate the accumulated charge states at molecular and atomic levels during cell operation. With the time increase of solar irradiation, multiple ESR signals were observed and the ESR intensities of all the PTzBT cells increased in low magnetic fields at around 321.5 mT regardless of with or without ITIC. Interestingly, the ESR intensity increased first then decreased in high magnetic fields at around 327.5 mT. The ESR measurements with layered films of PTzBT binary and ternary blend PSCs and their fitting analyses in the low magnetic fields at around 321.5 mT show several ESR signals which are assignable to holes in PTzBT, electrons on PC$_{61}$BM, and holes in ZnO, respectively. The accumulation of electrons on PC$_{61}$BM and holes in ZnO mainly

[1]Division of Materials Science, University of Tsukuba, Tsukuba, Ibaraki 305-8573, Japan. [2]Graduate School of Advanced Science and Engineering, Hiroshima University, Higashihiroshima, Hiroshima 739-8527, Japan. [3]Tsukuba Research Center for Energy Materials Science (TREMS), University of Tsukuba, Tsukuba, Ibaraki 305-8571, Japan. ✉email: marumoto@ims.tsukuba.ac.jp
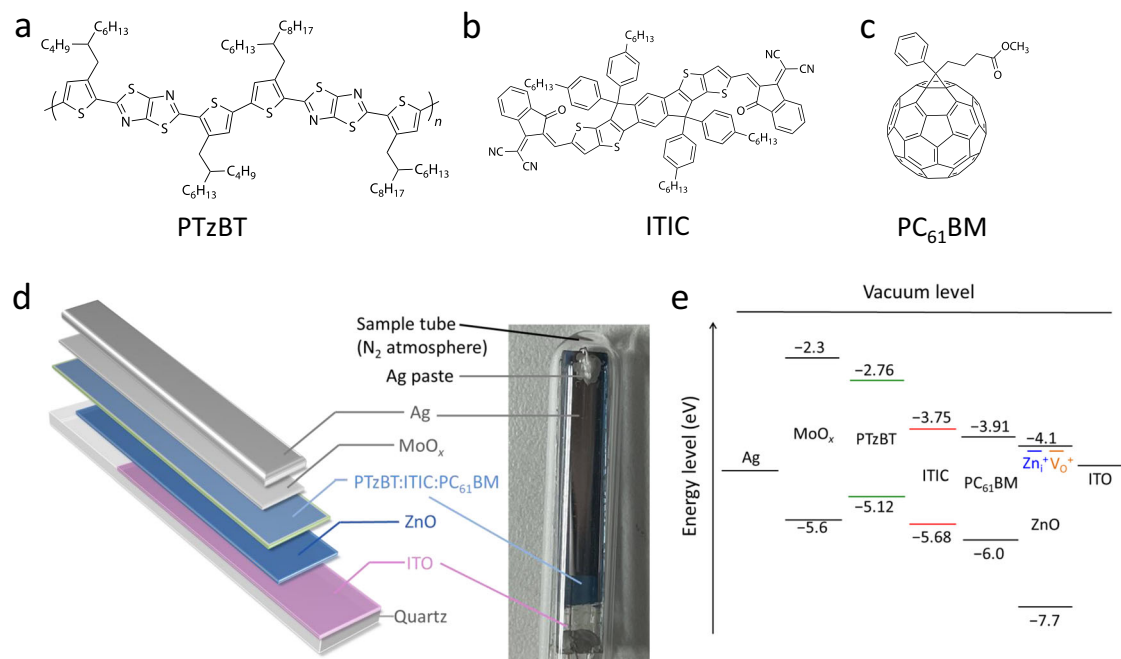
Fig. 1 **Chemical structures, device structure, and energy-level diagram of PTzBT polymer solar cells. a–c** Chemical structures of PTzBT, ITIC, and PC$_{61}$BM, respectively. **d** Device structure of a PTzBT ternary solar cell with ITIC and wiring details in a N$_2$-filled sample tube. **e** Energy diagram of the PTzBT cell (ITO/ZnO/PTzBT:ITIC:PC$_{61}$BM/MoO$_x$/Ag).

contributes to the deterioration of device performance. Furthermore, the ITIC addition to the PTzBT:PC$_{61}$BM binary blend PSCs reduces the charge accumulation of electrons on PC$_{61}$BM and holes in PTzBT, which leads to the less decrease in short-circuit current density of the cells. In addition, the correlation between the increase in open-circuit voltage and the decrease in accumulated holes in ZnO have been observed regardless of with or without ITIC addition, which is due to less vacuum level shift at the device interface. This deep clarification of the ternary blend PSCs will be essential for optimizing the cell structures and enhancing the PCE and stability of the cells.

RESULTS AND DISCUSSION
Operando ESR measurements of polymer solar cells
The ternary blend PSCs (ITO/ZnO/PTzBT:ITIC:PC$_{61}$BM/MoO$_x$/Ag) were fabricated with PTzBT, ITIC, and PC$_{61}$BM (Fig. 1d). The ESR signals and performance of the fabricated cells were simultaneously measured for the conditions of dark or solar irradiation by AM1.5 G, 100 mW cm^{-2} solar simulator (OTENTOSUN-150LX). The energy-level diagram of the PTzBT cell is show in Fig. 1e, whose energy values are taken from the literatures for ZnO and MoO$_x$ (ref. [25]), PTzBT and ITIC[8], PC$_{61}$BM[26], holes of singly charged zinc interstitial (Zn$_i^+$) and oxygen vacancy (V$_O^+$) in ZnO (ref. [27]), respectively.

ESR experiments were conducted using an X-band spectrometer (JEOL RESONANCE, JES-FA200) with a 1.0 mW microwave power at the center of the resonator. The cells and thin films were measured at the center of the ESR cavity. A continuous-wave ESR method with a lock-in detection for an external magnetic field H with a 100 kHz modulation frequency was utilized. Consequently, we cannot observe the light-induced charges with a short lifetime (<10 μs) which contribute to standard cell operation, and can only observe the charges accompanied with spins with a long lifetime (≥10 μs) in cells[9–12]. The solar cells or thin films and a standard Mn^{2+} marker were simultaneously measured in the same ESR cavity to directly compare these obtained ESR parameters. The g factor was calibrated by an ESR software considering high

second-order correction of the effective resonance field. We also used another standard sample 2,2-diphenyl-1-picrylhydrazyl (DPPH) to confirm the correctness of the g factor. Since the fluctuation of microwave power etc. can be calibrated by the marker's signals, the present ESR system remarkably decreases experimental errors. In our study, the H was parallel to the substrate plane unless otherwise stated. All the ESR signals were averaged over 1 h. When the cell's electrodes are in the cavity resonator, the occurrence of dielectric loss due to the electrodes causes a decrease of about 25% of the Q values of the cavity resonator. However, the impact is calibrated using the ESR intensity of the Mn^{2+} marker. During the ESR measurements, the microwave frequency and the ESR signal of the Mn^{2+} marker were measured simultaneously, and it was confirmed that all ESR signals were adjusted to the same microwave frequency.

Operando ESR signals of PTzBT cells with and without ITIC under device operation
Figure 2a, b show the operando ESR spectra of the PTzBT cells with/without ITIC under short-circuit conditions and Fig. 2c, d show those under open-circuit conditions, respectively. In the dark conditions, all the cells show one ESR signal where the ESR parameters are g factor $g = 2.0024(\pm0.0002)$ and peak-to-peak ESR linewidth $\Delta H_{pp} = 0.16(\pm0.02)$ mT. The g factors are calculated by the resonant magnetic field. We calibrated the ESR parameters by the Mn^{2+} marker. The axes of ordinates are plotted with a unit of a peak-to-peak ESR intensity of the Mn^{2+} marker (I_{Mn}). As the duration of solar irradiation increased, multiple ESR signals were observed and the ESR intensities of all the cells regardless of with or without ITIC increased in the low magnetic fields at around 321.5 mT, respectively. Interestingly, the ESR intensity in the high magnetic fields at around 327.5 mT increased when the solar light was irradiated for 1 h, and then decreased gradually with time, which indicated that the N_{spin} first increased and then decreased under solar irradiation (Fig. 2c, d). Investigation of the origins for these charge-accumulation states are essential for clarifying the mechanisms of performance improvement and internal deterioration. Thin films of PTzBT:ITIC:PC$_{61}$BM, PTzBT:PC$_{61}$BM, ZnO, ITIC, and
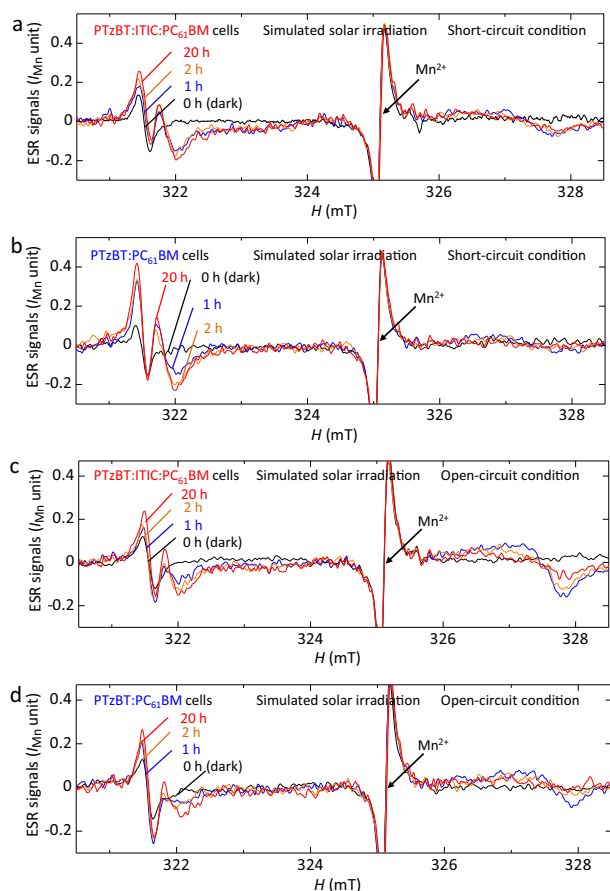
Fig. 2 **Operando ESR signals of PTzBT cells with and without ITIC.** **a–d** Time variation of operando ESR spectra of PTzBT cells (**a**, **c**) with and (**b**, **d**) without ITIC under solar irradiation under (**a**, **b**) short- and (**c**, **d**) open-circuit conditions at room temperature, respectively. The substrate planes are parallel to the direction of external magnetic field H.

MoO$_x$, and PC$_{61}$BM and PC$_{71}$BM films on the ZnO layer (ZnO/PC$_{61}$BM and ZnO/PC$_{71}$BM) were fabricated and investigated to clarify the origins of these ESR spectra of the cells.

Identification of cation signal of PTzBT (Signal 1)

Figure 3a shows the ESR spectra of the PTzBT:ITIC:PC$_{61}$BM and PTzBT:PC$_{61}$BM thin films under solar irradiation. Under dark conditions, no signal has been observed for these thin films. Under solar irradiation, the above two thin films exhibited same ESR signals where the ESR parameters are $g_1 = 2.0023 \pm 0.0002$ and $\Delta H_{pp1} = 0.16 \pm 0.02$ mT. An ESR signal of ITIC was not observed in both the PTzBT:ITIC:PC$_{61}$BM and PTzBT:PC$_{61}$BM thin films because the same ESR spectra were obtained. Furthermore, almost no signal was observed for ITIC thin film under the dark and irradiation conditions (Supplementary Fig. 3a). Under simulated solar irradiation, excitons are generated by solar irradiation and separated at the interface between PTzBT and PC$_{61}$BM. Thus, the cation signal of PTzBT and the anion signal of PC$_{61}$BM can be observed. Since the spectrum of PC$_{61}$BM anion cannot be observed at room temperature due to the short spin-lattice relaxation time[9–12], the obtained ESR spectrum is confirmed as a cation (or hole) signal of PTzBT. The cation signal of PTzBT in PTzBT:ITIC:PC$_{61}$BM film is larger than that in PTzBT:PC$_{61}$BM film, which suggests that ITIC can promote the charge separation and enhance the cation (or hole) formation in PTzBT.
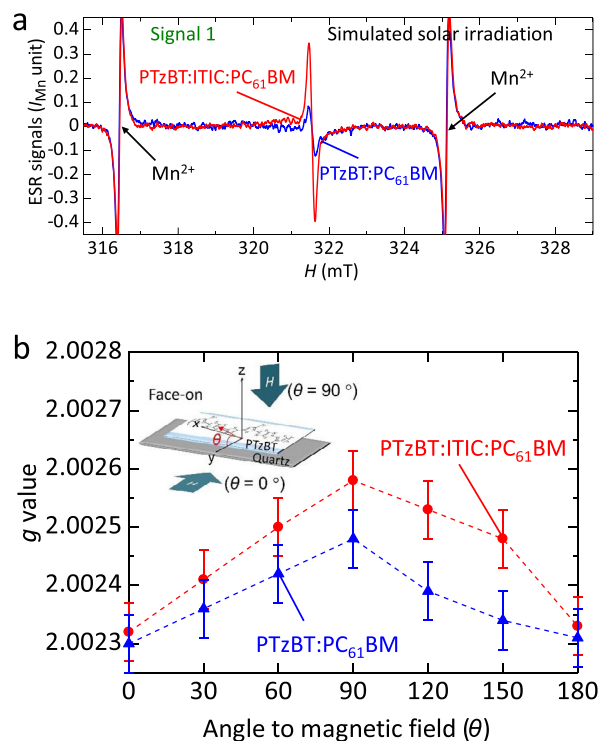

Fig. 3 **ESR signals of thin films of PTzBT:ITIC:PC$_{61}$BM and PTzBT:PC$_{61}$BM, and the anisotropy measurements.** **a** ESR spectra of thin films of PTzBT:ITIC:PC$_{61}$BM (red line) and PTzBT:PC$_{61}$BM (blue line) (defined as Signal 1) after 20 h solar irradiation. **b** Anisotropies of the ESR signals of the PTzBT:ITIC:PC$_{61}$BM and PTzBT:PC$_{61}$BM thin films measured by changing the angle θ between the substrate plane and H direction. The error bars are ±0.00005.

The ESR parameters of the Signal 1 accord with those of the cell's signals under dark conditions (Fig. 2). This indicates that the cations (or holes) in PTzBT formed in the cells are due to the hole transfer from MoO$_x$ under dark conditions because the energy level of the valence band of MoO$_x$ has been reported approximately −5.6 eV[25,28], which is deeper than that of the highest occupied molecular orbital (HOMO) of PTzBT (−5.12 eV) (Fig. 1e)[8].

Since polymer orientation plays a crucial role in device performance and stability, we studied the orientation in the PTzBT:ITIC:PC$_{61}$BM and PTzBT:PC$_{61}$BM thin films by observing the anisotropy of the ESR signal of PTzBT (Signal 1) with changing the angle θ between the substrate plane and H direction (Fig. 3b). The anisotropy of the g factor is observed as $g = 2.00233 \pm 0.00005$ at $\theta = 0°$ and $g = 2.00258 \pm 0.00005$ at $\theta = 90°$ for the PTzBT:ITIC:PC$_{61}$BM thin film, which is larger than that for the PTzBT:PC$_{61}$BM thin film. The results directly show the ITIC addition can enhance the molecular orientation of PTzBT with hole accumulation in the active layer.

To get more accurate anisotropy of the PTzBT molecular orientation with accumulated holes (Signal 1), we conducted density functional theory (DFT) calculation using Gaussian 16W[10,11,18,29]. The g-factor shift can be used to determine whether charges are accumulated at polymer-chain ends. It has been reported that residual bromine exists on polymer-chain ends in conducting polymers, such as P3HT[18,29], PTB7[10], and PTB7-Th[11], even if the chain-end treatment is conducted. Thus, the model molecules of PTzBT with residual bromine-end (monomer, dimer, and trimer defined as TzBT-Br, 2TzBT-Br, and 3TzBT-Br, respectively) and of PTzBT without residual bromine-end (monomer, dimer, and trimer defined as TzBT-H, 2TzBT-H, and 3TzBT-H, respectively) were calculated using 6-31 G(d,p) basis set and
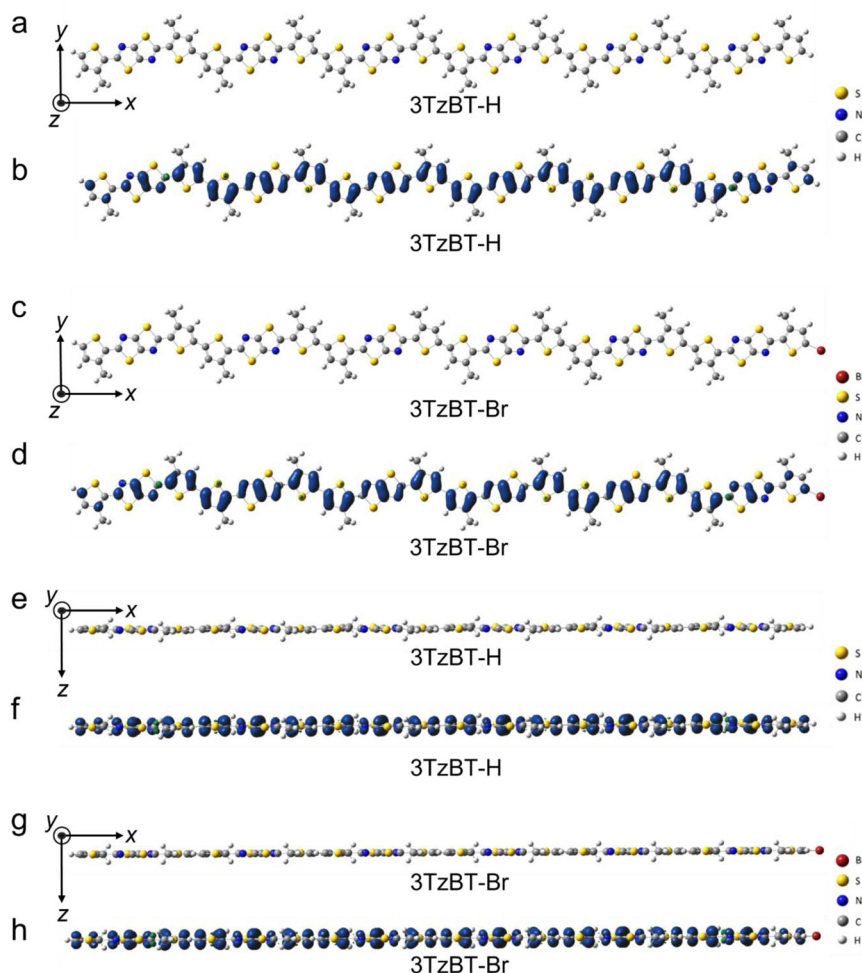
Fig. 4 Model molecules for DFT calculation and spin density distribution in cationic states. a, c Model molecules of PTzBT trimers for the DFT calculation: **a** 3TzBT-H, **c** 3TzBT-Br. **b, d** Spin density distribution in cationic states: **b** 3TzBT-H, **d** 3TzBT-Br. **e, g** Side views of model molecules of PTzBT trimers for the DFT calculation: **e** 3TzBT-H, **g** 3TzBT-Br. **f, h** Side views of spin density distribution in cationic states: **f** 3TzBT-H, **h** 3TzBT-Br.

UB3LYP functional. The optimized chemical structures of the PTzBT model trimers and the spin density distribution in cationic states are shown in Fig. 4, where the coordinate axes of x, y, and z-axis are defined as the long, short, and molecular-plane-perpendicular axis of the molecule, respectively. As shown in Fig. 4e–h, the side views of the optimized chemical structures and spin density distribution obtained from the DFT calculation show good coplanarity in the cationic states, respectively. Supplementary Figs. 1 and 2 show the chemical structures of the model dimers and monomers with their spin density distribution in cationic states, respectively. Table 1 summarizes the DFT results of all model molecules. The averaged g factors ($g_{\mu v}$) can be calculated with a root mean square of principal values of g tensors g_μ and g_v (μ, $v = x, y, z$) as follows:

$$g_{\mu v} = \sqrt{\frac{g_\mu^2 + g_v^2}{2}}, (\mu, v = x, y, z).\tag{1}$$

Since the g factors of the monomer model-molecule TzBT-Br are so large that they cannot explain the observed g factors, we focus on other g factors. According to the DFT calculation (Table 1), g_y of all the model molecules are larger than other calculated g factors. Thus, the observed large g factor at $\theta = 90°$ ($g = 2.00258$) can be

described by the g_y. Thus, the orientation of molecules with charge accumulation is found to be "edge-on", that is, the molecular plane is perpendicular to the substrate plane, which is inconsistent with the previous study of two-dimensional grazing incidence X-ray diffraction (2D-GIXD) (see the inset of Fig. 3b)[8,30]. The reason is thought to be that the accumulated charges are not in the main face-on orientation area but in the edge-on orientation area of PTzBT. Although the g_y of 2TzBT-H ($g_y = 2.00258$) and 3TzBT-H ($g_y = 2.00260$) accord with the observed g factor at $\theta = 90°$ ($g = 2.00258$), the g_{xz} of 2TzBT-H ($g_{xz} = 2.00169$) and 3TzBT-H ($g_{xz} = 2.00176$) are much smaller than the observed g factor at $\theta = 0°$ ($g = 2.00233$) (Table 1). Consequently, the cations (or holes) may accumulate in the regions with molecular structures similar to TzBT-H, 2TzBT-Br, and 3TzBT-Br under solar irradiation. Since the observed g factor at $\theta = 90°$ ($g = 2.002583$) are smaller than the calculated g_y of TzBT-H ($g_y = 2.00277$), 2TzBT-Br ($g_y = 2.00315$), and 3TzBT-Br ($g_y = 2.00292$), and that at $\theta = 0°$ ($g = 2.00233$) are larger than the calculated g_{xz} of TzBT-H ($g_{xz} = 2.00165$), 2TzBT-Br ($g_{xz} = 2.00199$), and 3TzBT-Br ($g_{xz} = 2.00194$) (see Table 1), the molecular orientation is not a perfect edge-on orientation and the y-axis direction tilt from the normal direction of the substrate plane. As a result, PTzBT have a slightly disordered molecular orientation and the hole accumulation is thought to exist near the chain ends of PTzBT.

Table 1.	Calculated *g*-tensors' principal values and their averaged values of model molecules of PTzBT with and without bromine end.						
Molecule	Length	g_x	g_y	g_z	g_{xy}	g_{xz}	g_{yz}
TzBT-H	Monomer	2.00118	2.00277	2.00211	2.00198	2.00165	2.00244
2TzBT-H	Dimer	2.00127	2.00258	2.00210	2.00193	2.00169	2.00234
3TzBT-H	Trimer	2.00142	2.00260	2.00210	2.00201	2.00176	2.00235
TzBT-Br	Monomer	2.00295	2.00491	2.00186	2.00393	2.00241	2.00339
2TzBT-Br	Dimer	2.00195	2.00315	2.00202	2.00255	2.00199	2.00259
3TzBT-Br	Trimer	2.00182	2.00292	2.00205	2.00237	2.00194	2.00248

Identification of anion signal of PC₆₁BM (Signal 2) and hole signal of singly charged oxygen vacancy in ZnO (Signal 3)

To identify other origins of observed ESR signals except for the Signal 1 related with PTzBT, thin films of ZnO/PC$_{61}$BM, ZnO/PC$_{71}$BM, and ZnO were also measured under solar irradiation. The ESR spectra of the ZnO/PC$_{61}$BM film under dark condition, where no signal was observed, and 1 h and 20 h under solar irradiation are shown in Fig. 5a. Multiple ESR signals were observed and the ESR intensity in the low magnetic fields at around 321.5 mT increased with irradiation time. On the other hand, the ESR intensity in the high magnetic fields at around 327.5 mT increased at 1 h, then decreased at 20 h. Such signal changes are similar to those observed in the cells as shown in Fig. 2. We performed a least-squares fitting analysis using EasySpin (6.0.0-dev.17) and Igor Pro (6.36 J) to find out the components of the ESR signals for the ZnO/PC$_{61}$BM film in the low magnetic fields at around 321.5 mT. Figure 5b shows the fitting analysis of the ESR spectrum for the ZnO/PC$_{61}$BM film obtained after 20 h solar irradiation. The results are evaluated as follows: The component of the ESR signal, whose lineshape is Lorentzian type and ESR parameters are $g_2 = 2.0004 \pm 0.0008$ and $\Delta H_{pp2} = 0.34 \pm 0.02$ mT, is defined as "Signal 2". The component of the ESR signal, whose lineshape is Lorentzian type and ESR parameters are $g_3 = 2.0027 \pm 0.0002$ and $\Delta H_{pp3} = 0.21 \pm 0.02$ mT, is defined as "Signal 3".

The *g* factor of the Signal 2 (g_2) is similar to the previously calculated *g* factor for an anion of PC$_{61}$BM using a DFT method[31]. We infer that the Signal 2 is an anion signal of PC$_{61}$BM. To get more accurate identification of the Signal 2, the ZnO/PC$_{71}$BM film was measured under the same condition used for the ZnO/PC$_{61}$BM film. Supplementary Fig. 3 shows the ESR signals of the ZnO/PC$_{71}$BM film. The Signal 2 is found to be the anion signal of PC$_{61}$BM because the Signal 2 cannot be observed when PC$_{71}$BM is layered on ZnO (Supplementary Fig. 3b). Thus, we conclude that the Signal 2 (anion signal of PC$_{61}$BM) can be observed under solar irradiation when PC$_{61}$BM is layered on ZnO. Since PC$_{61}$BM anions in the active layer cannot be observed at room temperature due to the short spin-lattice relaxation time as mentioned above[9–12], the ESR observation of PC$_{61}$BM anions at room temperature indicates the direct interaction of PC$_{61}$BM with ZnO, suggesting a mixing of wave function between PC$_{61}$BM and ZnO. This interaction may enable the ESR observation of PC$_{61}$BM anions by breaking the symmetry of electron wave function on PC$_{61}$BM, resulting in the long spin-relaxation time. Thus, the electron accumulation on PC$_{61}$BM is thought to occur at the PC$_{61}$BM/ZnO interface. In previous studies, the Signal 3 has been reported as the hole signal of singly charged oxygen vacancies in ZnO (V$_O^+$ signal)[32]. We have observed the Signal 3 ($g = 2.0027 \pm 0.0002$) in the ESR measurements of both ZnO/PC$_{61}$BM and ZnO/PC$_{71}$BM films (Supplementary Fig. 3). Therefore, the Signal 2 and Signal 3 are identified as the PC$_{61}$BM anion signal and the hole signal of ZnO (V$_O^+$ signal), respectively.
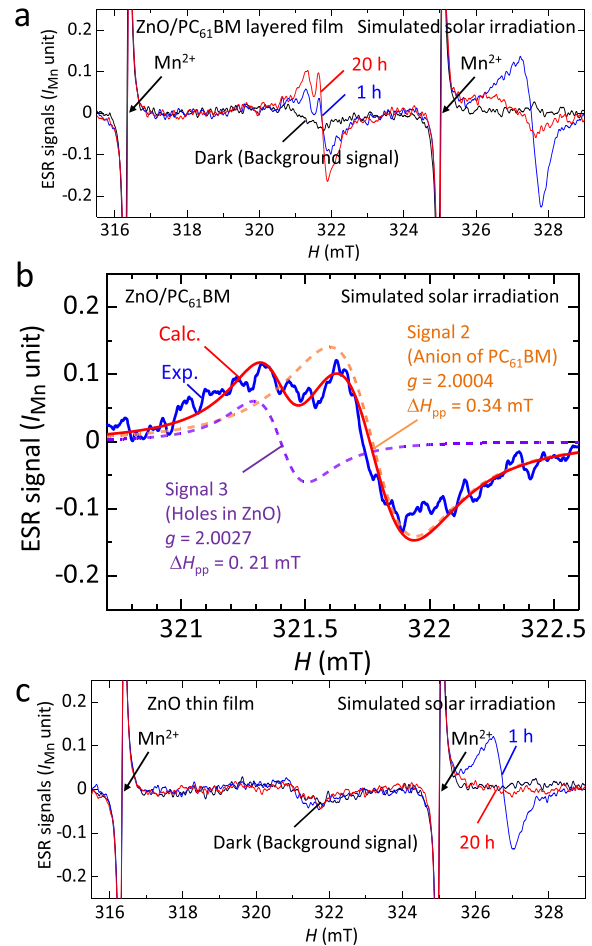

Fig. 5 ESR signals of ZnO/PC$_{61}$BM layered film and ZnO thin film and fitting analysis. a Time variation of ESR spectra of ZnO/PC$_{61}$BM layered film. b Fitting analysis for the ZnO/PC$_{61}$BM signal in low magnetic fields at around 321.5 mT (Signal 2 and Signal 3). c Time variation of ESR spectra of ZnO thin film in high magnetic fields at around 327.5 mT (Signal 4). These samples were measured with the same conditions used for the cells.

Identification of hole signal of singly charged zinc interstitial in ZnO (Signal 4)

To identify the ESR signal of the cells in the high magnetic fields at around 327.5 mT (Fig. 2), we studied the ZnO thin film using ESR spectroscopy (Fig. 5c). We define the obtained ESR signal, whose ESR parameters are $g_4 = 1.9697$ (±0.005) and $\Delta H_{pp4} = 0.54$(±0.02) mT, as Signal 4. The ESR parameters and the ESR intensity change accord with those of the cells in the high magnetic fields at around 327.5 mT (Fig. 2). In previous studies, the signal with $g \approx 1.96$ has been identified as the hole signal of singly charged zinc
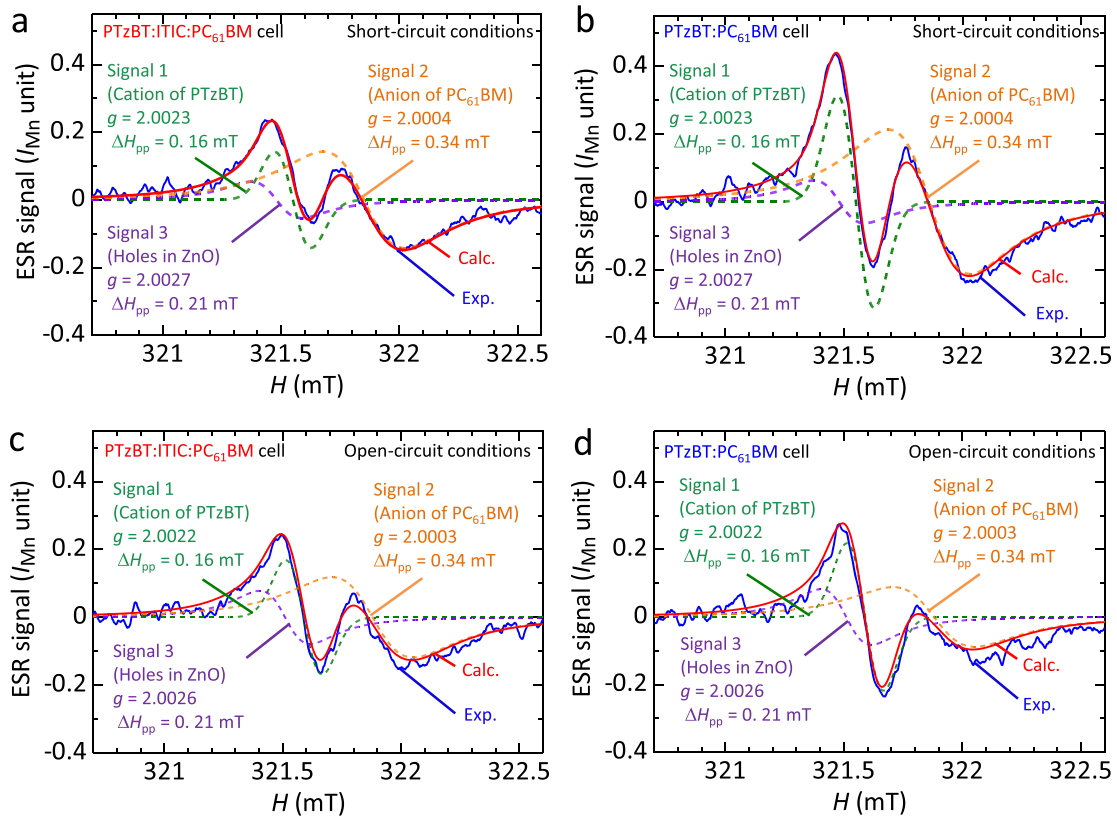
Fig. 6   Fitting analyses of the operando ESR signals of the PTzBT cells after 20 h solar irradiation. a–d Fitting analyses of the ESR signals of the PTzBT cells (**a**, **c**) with and (**b**, **d**) without ITIC under (**a**, **b**) short- and (**c**, **d**) open-circuit conditions in low magnetic fields at around 321.5 mT, respectively. Red lines represent the sum of green dotted line (Signal 1, cation of PTzBT), orange dotted line (Signal 2, anion of $PC_{61}BM$), and purple dotted line (Signal 3, holes in ZnO (V_O^+)).

interstitials in ZnO (Zn_i^+ signal) (ref. [32]). This g factor is consistent with that of the Signal 4. Thus, the origin of the Signal 4 is assigned to the hole signal of singly charged zinc interstitials in ZnO (Zn_i^+ signal) (ref. [32]). Immediately after solar irradiation, a large number of holes were suddenly trapped in zinc interstitials, where zinc interstitials can be formed by solar irradiation with short wavelengths (Frenkel reaction[27]), and the Signal 4 (Zn_i^+ signal) of the ZnO thin film first greatly increased. After that, during solar irradiation, the Signal 4 (Zn_i^+ signal) of the ZnO thin film decreased with the time increase of solar irradiation, which indicates that the accumulated charges are detrapped by solar irradiation. The reason for this detrapping is thought to be the recombination between Zn_i^+ and electrons generated by solar irradiation with short wavelengths. We can assume the same mechanism occurs for the cells' signal in Fig. 2 because of the same behavior of the Signal 4. Thus, the N_{spin} of the cells (Fig. 2) first increases then decreases at 327.5 mT.

We also measured the MoO_x thin film to confirm the ESR signal of oxygen vacancy in MoO_x and hyperfine structures from Mo and its isotopes. As a result, almost no signal was observed under dark and irradiation conditions (Supplementary Fig. 3c). Thus, MoO_x has no effect on the identifications of the ESR signals of the cells.

Fitting analyses of the operando ESR signals for PTzBT cells

Least-squares fitting analyses were further performed to identify the components of the operando ESR signals for the cells obtained after 20 h solar irradiation in the low magnetic fields at around 321.5 mT (Fig. 2). After having tried various functions based on the ESR parameters of the Signal 1, 2, and 3, the sum of one Gaussian and two Lorentzian functions shows the best results for each

operando ESR spectrum as shown in Fig. 6. Similar component signals have been obtained using the fitting analyses under short- (Fig. 6a, b) and open-circuit conditions (Fig. 6c, d) regardless of with or without ITIC, respectively. Table 2 summarizes the fitting analysis results. From the results, the same components have been identified under short- and open-circuit conditions, respectively.

Correlations between operando ESR signals and device performance

It is essential to clarify the correlation between the device performance and the number of spins (N_{spin}) that corresponds to the number of accumulated charges in the cells. For this purpose, the device performance (Supplementary Fig. 4) and ESR signals were simultaneously measured in solar irradiation, and their correlations were analyzed. The standard Mn^{2+} marker sample was used to calculate the N_{spin}. Figure 7a, b show the transient responses of the relative short-circuit current density ($J_{SC}(t)/J_{SC}(0)$) and the calculated N_{spin} in the low magnetic fields at around 321.5 mT from the signals of the cells with and without ITIC, respectively, where $J_{SC}(t)$ is normalized to the initial value of $J_{SC}(0)$ at irradiation time $t = 0$. A clear correlation is observed between the $J_{SC}(t)/J_{SC}(0)$ decrease and the N_{spin} increase in the low magnetic fields at around 321.5 mT under solar irradiation, as reported in the ESR researches of other polymer solar cells[9–12].

The transient responses of the N_{spin} of the Signal 1, Signal 2, and Signal 3 upon solar irradiation are shown by Green rhombus, orange triangles, and purple squares in Fig. 7a, b, respectively. The total N_{spin} corresponds to the sum of these three components. The N_{spin} for the Signal 1, Signal 2, and Signal 3 were calculated by the deconvolution of the ESR signals by the fitting analyzes

Table 2. Results of fitting analyses of g factors and ΔH_{pp} of Signal 1, Signal 2, and Signal 3 of PTzBT solar cells with and without ITIC under short- or open-circuit conditions.

PTzBT cell	Signal	Lineshape	Short-circuit condition		Open-circuit condition	
			g factor	ΔH_{pp} (mT)	g factor	ΔH_{pp} (mT)
w/ ITIC	Signal 1	Gaussian	2.0023 ± 0.0002	0.16 ± 0.02	2.0023 ± 0.0002	0.16 ± 0.02
	Signal 2	Lorentzian	2.0004 ± 0.0002	0.34 ± 0.02	2.0004 ± 0.0002	0.34 ± 0.02
	Signal 3	Lorentzian	2.0027 ± 0.0002	0.21 ± 0.02	2.0027 ± 0.0002	0.21 ± 0.02
w/o ITIC	Signal 1	Gaussian	2.0022 ± 0.0002	0.16 ± 0.02	2.0022 ± 0.0002	0.16 ± 0.02
	Signal 2	Lorentzian	2.0003 ± 0.0002	0.34 ± 0.02	2.0003 ± 0.0002	0.34 ± 0.02
	Signal 3	Lorentzian	2.0026 ± 0.0002	0.21 ± 0.02	2.0026 ± 0.0002	0.21 ± 0.02
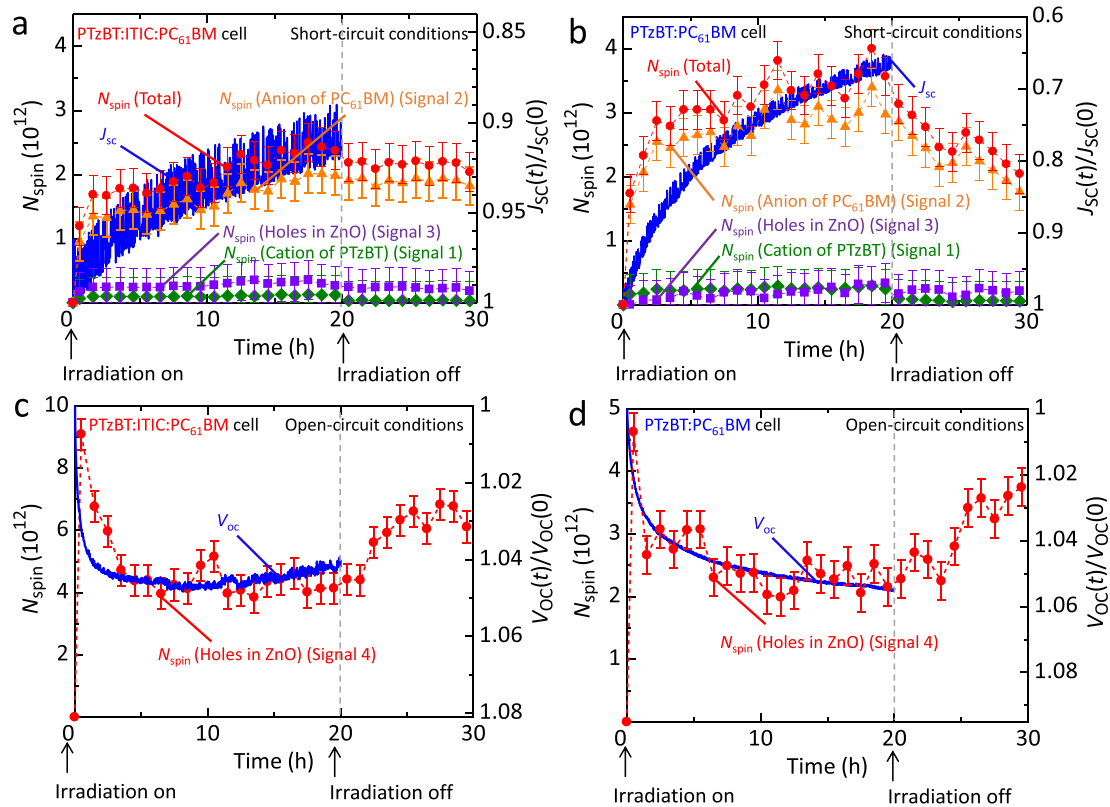
Fig. 7 Time variation of the N_{spin} of PTzBT cells and device performance. a–d Time variation of the N_{spin} (red circles) and (**a, b**) J_{SC} (t)/J_{SC} (0) (blue line) or (**c, d**) V_{OC} (t)/V_{OC} (0) (blue line) for the cells (**a, c**) with and (**b, d**) without ITIC under solar irradiation at room temperature, respectively. Here, $J_{SC}(t)$ and $V_{OC}(t)$ are normalized to their initial values of $J_{SC}(0)$ and $V_{OC}(0)$ at irradiation time $t = 0$, respectively. The N_{spin} are plotted at each averaged time over 1 h. The error bars in **a, b, d** and in **c** are ±0.3 × 10^{12} and ±0.5 × 10^{12}, respectively.

shown in Fig. 6. The N_{spin} of the Signal 2 dominates the total N_{spin}. The N_{spin} of the Signal 3 shows the similar transient response regardless of with or without ITIC (Fig. 7a, b). However, the N_{spin} for the Signal 1 and Signal 2 for the cell with ITIC are obviously smaller than those of the cell without ITIC (Fig. 7a, b). The transient responses of the relative open-circuit voltage ($V_{OC}(t)/V_{OC}(0)$) and the N_{spin} in the high magnetic fields at around 327.5 mT obtained from the cells with and without ITIC are shown in Fig. 7c, d, respectively, where $V_{OC}(t)$ is normalized to the initial value of $V_{OC}(0)$ at $t = 0$. For this case, we observe another correlation between the increase in $V_{OC}(t)/V_{OC}(0)$ and the decrease in the N_{spin} of the Signal 4 (hole signal of ZnO (Zn_i^+)) under solar irradiation from 1 h to 20 h regardless of with or without ITIC as shown in

Fig. 7c, d, respectively. The above two correlations for the $J_{SC}(t)/J_{SC}(0)$ and $V_{OC}(t)/V_{OC}(0)$ cases are further discussed below.

Performance improvement and deterioration mechanisms of PTzBT solar cells

On the basis of the correlations between device performance and N_{spin} mentioned above, we discuss the mechanisms of the performance improvement and deterioration of the cells. In the case of cells with charge accumulation, the J_{SC} can be described as follows[9–12]:

$$J_{SC}\left(N_{spin}\right) = ne\mu E = ne\frac{\mu_{SC}\mu_{CA}}{\mu_{CA} + (\mu_{SC}/c)N_{spin}}E. \quad (2)$$

Here, n is charge density, e is elementary charge, μ is the mobility of Matthiessen's rule, E is internal electric field, μ_{SC} and μ_{CA} are the mobilities without and with charge accumulation, and c is a proportional constant[9–12]. From Eq. (2), the $J_{SC}(0)$ can be calculated, which derives $J_{SC}(N_{spin})/J_{SC}(0)$ as follows[9–12]:

$$\frac{J_{SC}(N_{spin})}{J_{SC}(0)} = \frac{\mu_{CA}}{\mu_{CA} + (\mu_{SC}/c)N_{spin}} = \frac{1}{1 + \left(\frac{\mu_{SC}}{c \cdot \mu_{CA}}\right)N_{spin}}. \quad (3)$$

Equation (3) shows that the J_{SC} decreases while the N_{spin} increases, as observed in Fig. 7a, b. The collision time of charge carriers, and thus their mobility, in the PTzBT cells with and without ITIC decreases because of the scattering of charge carriers by accumulated charges under solar irradiation. This deterioration mechanism is the same as that reported for other polymer solar cells[9–12].

Compared to the PTzBT cell without ITIC, the PTzBT cell with ITIC was found to have less hole accumulation in PTzBT and less electron accumulation on $PC_{61}BM$. In the case of holes in PTzBT, the probability of the hole carriers going to the chain ends of PTzBT is thought to be reduced because the ITIC addition enhances the molecular orientation and thus enhances the hole transport between stacked PTzBT molecules with π-π stacking interaction in the active layer (Fig. 3b), which prevents the hole traps at chain ends and thus leads to the less hole accumulation in PTzBT. The enhancement of the molecular orientation of PTzBT have been confirmed by GIWAXS (or GIXD) in the previous study (Fig. S11 of ref. [8]). The intensities of the PTzBT:$PC_{61}BM$ blend film with ITIC (more than 0 wt%) at $q_{xy} = 0.35$ are larger than that without ITIC (0 wt%) (Fig. S11b of ref. [8]). However, the intensities at $q_z = 0.35$ are almost same regardless of with or without ITIC addition (Fig. S11a of ref. [8]). The larger ratio of q_{xy} to q_z means more molecular orientation of PTzBT. Thus, the ITIC addition can enhance the molecular orientation of PTzBT, which corresponds to the observed PTzBT anisotropy in the ESR measurements (Fig. 3b).

The ITIC molecules can co-exist with $PC_{61}BM$ molecules because the surface energies of ITIC (31.2 mJ m^{-2}) and $PC_{61}BM$ (33.3 mJ m^{-2}) are similar to each other[8]. Moreover, the ESR signal intensity of $PC_{61}BM$ anions in ZnO/ITIC:$PC_{61}BM$, which corresponds to the Signal 2, has been reported to be smaller than that of ZnO/$PC_{61}BM$, as shown in previous study[33], which indicates that the electron accumulation on $PC_{61}BM$ at the ZnO interface is reduced by the ITIC addition. As discussed above, the electron accumulation on $PC_{61}BM$ is thought to occur at the ZnO/$PC_{61}BM$ interface. Consequently, a part of the ITIC aggregations maybe directly contacts with the ZnO layer and thus some electrons can directly transfer from ITIC to the ZnO layer, which reduces the electron accumulation on $PC_{61}BM$ at the ZnO interface. Thus, the ITIC addition in the active layer causes the less N_{spin} of holes in PTzBT and electrons on $PC_{61}BM$, which leads to the less decrease in the $J_{SC}(t)/J_{SC}(0)$ of the cells. Although the ITIC addition can reduce the electron accumulation on $PC_{61}BM$, we still observe a lot of electrons accumulated on $PC_{61}BM$. From our results, $PC_{61}BM$ is not a very ideal n-type material for PSCs because a large number of electrons are accumulated on $PC_{61}BM$ during device operation, which deteriorates the device stability. To improve the stability of the cells, it is essential to reduce the charge accumulation in the active layer during device operation.

Next, the reason of the correlation between the increase in $V_{OC}(t)/V_{OC}(0)$ and the decrease in the N_{spin} of the Signal 4 (hole signal of ZnO (Zn_i^+)) regardless of with or without ITIC is discussed. As shown in Fig. 7c, d, the $V_{OC}(t)/V_{OC}(0)$ increased as the duration of solar irradiation increased. According to the theoretical study, the V_{OC} of organic solar cells has been reported to be evaluated as follows[34]:

$$V_{OC} = |HOMO_D| - |LUMO_A| + BB_D + BB_A - \Delta\Phi_D - \Delta\Phi_A. \quad (4)$$

Here, $|HOMO_D| - |LUMO_A|$ is the energy difference between the HOMO of the donor and the lowest unoccupied molecular orbital (LUMO) of the acceptor, BB_D and BB_A are the net band bendings in the electrostatic potential, and $\Delta\Phi_D$ and $\Delta\Phi_A$ are the energy offsets at the contact[34]. In previous ESR studies, electrons and holes have been reported to be accumulated, which form an electric dipole layer at the interface between a hole transport layer (HTL) poly(3,4-ethylenedioxythiophene):pol(4-styrenesulfonate) (PEDOT:PSS) and an active layer such as P3HT, PTB7, and PTB7-Th under solar irradiation[9–12]. These charge-accumulation states can lead to the occurrence of energy-level shift and the variance of the $\Delta\Phi_D$. With the time increase of solar irradiation, the N_{spin} of holes in P3HT, PTB7, or PTB7-Th (active layer) and electrons in PEDOT:PSS (HTL) increases, which contributes to the increase in the $\Delta\Phi_D$ and leads to the decrease in the V_{OC} of those cells[9–12]. In the present case of the PTzBT cells, electrons and holes mainly accumulate on $PC_{61}BM$ (active layer) and in ZnO (electron transport layer (ETL)) under solar irradiation, respectively. These charge-accumulation states lead to the variation of the $\Delta\Phi_A$, which is different from the above cases of the P3HT, PTB7, or PTB7-Th cells.

From Fig. 7a–d, we find that electrons on $PC_{61}BM$ (Signal 2) and holes in ZnO (Zn_i^+, Signal 4) dominant the N_{spin} of the cells,
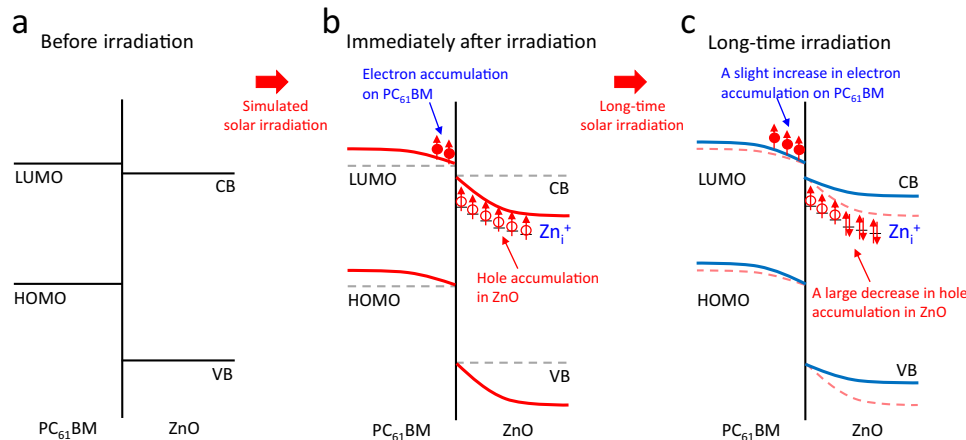

Fig. 8 Schematic variation of the interface energy level between $PC_{61}BM$ and ZnO under solar irradiation. a Before solar irradiation, electrons and holes are not trapped on $PC_{61}BM$ and in ZnO so the anion signal of $PC_{61}BM$ (Signal 2) and the hole signal of ZnO (Zn_i^+ signal, Signal 4) are not observed. **b** Immediately after solar irradiation, a large number of electrons and holes are suddenly trapped at the interface between $PC_{61}BM$ and ZnO layer. **c** After long-time solar irradiation, the N_{spin} of holes in ZnO (Signal 4) has massively decreased.

respectively. The hole and electron accumulation states at the interfaces between $PC_{61}BM$ and ZnO under open-circuit conditions are schematically shown in Fig. 8. Before solar irradiation (Fig. 8a), electrons on $PC_{61}BM$ and holes in ZnO are not trapped so we observe no anion signal of $PC_{61}BM$ (Signal 2) and no hole signal of ZnO (Zn_i^+ signal, Signal 4). Immediately after solar irradiation (Fig. 8b), a large number of electrons on $PC_{61}BM$ and holes in ZnO are suddenly trapped at the interface between $PC_{61}BM$ in the active layer and the ZnO layer, respectively, then the anion signal of $PC_{61}BM$ (Signal 2) and the hole signal of ZnO (Zn_i^+ signal, Signal 4) begin to be observed because of the Frenkel reaction[27] (Figs. 2 and 5a, b). The hole accumulation also can be confirmed by the cells' transient responses under open-circuit conditions (Fig. 7c, d). Along with the increases in electrons on $PC_{61}BM$ and holes in ZnO, the energy level of $PC_{61}BM$ near the interface become shallower and that of ZnO become deeper (Fig. 8b). This energy-level shift causes the $\Delta\Phi_A$ increase, which means that the performance deterioration due to the charge accumulation has already occurred at the time of the immediately after solar irradiation regardless of with or without ITIC. This sudden performance deterioration cannot be observed by usual device characterization measurements because they need to use solar irradiation to obtain the photovoltaic properties. Very interestingly, it should be noted that if the cells are irradiated for a long time (Fig. 8c), the N_{spin} of holes in ZnO (Signal 4) has massively decreased (Fig. 7c, d), which leads to a large decrease in the energy-level shift and causes the decrease in $\Delta\Phi_A$. In contrast to the slight increase of the N_{spin} of electrons on $PC_{61}BM$, the large decrease of the N_{spin} of ZnO partly recovers the energy-level shift between of the $PC_{61}BM$ and ZnO layers, which causes the $\Delta\Phi_A$ decrease and leads to the increase in the V_{OC}. This V_{OC} increase during device performance occurs the cells with and without ITIC, which indicates that the optimization of the trapping states in ZnO is very important for further improving the device performance, which can be demonstrated by the present operando ESR study of the cells.

In conclusion, the PTzBT PSCs with and without ITIC have been studied by operando ESR spectroscopy under solar irradiation. We have clarified the origins of four ESR components for the cells from the measurements of the thin films and the fitting analyses for the ESR signals, where the signal 1, 2, 3, and 4 are identified as the cation signal of PTzBT (Signal 1), the anion signal of $PC_{61}BM$ (Signal 2), the hole signal of singly charged oxygen vacancies in ZnO (V_O^+, Signal 3), and the hole signal of singly charged zinc interstitials in ZnO (Zn_i^+, Signal 4), respectively. With the time increase of solar irradiation, the intensities of the Signal 1, 2, and 3 increased monotonically, the intensity of the Signal 4 firstly increased then decreased regardless of with or without ITIC. From the ESR anisotropy measurements, we have found the ITIC addition can enhance the molecular orientation of PTzBT with hole accumulation in the active layer. We have observed the clear correlation of the $J_{SC}(t)/J_{SC}(0)$ decrease with the N_{spin} increase regardless of with or without ITIC, which has demonstrated that the charge scattering by accumulated charges lead to the decrease in charge-carrier mobility. The degree of the N_{spin} increase of the cells with ITIC is lower than that of those without ITIC because of the enhancement of the molecular orientation by ITIC and the direct contact between ZnO and ITIC, resulting in higher performance and stability for the cells with ITIC compared to those without ITIC. This result explains the stability improvement mechanism by the ITIC addition from a microscopic viewpoint. In addition, regardless of with or without ITIC addition, the correlation between the $V_{OC}(t)/V_{OC}(0)$ increase and the N_{spin} decrease has been also observed, which demonstrates that the decrease of hole accumulation in ZnO causes the $\Delta\Phi_A$ decrease and lead to the increase in the V_{OC}. From our findings, further decrease in the N_{spin} under device operation will be essential for the development of PSCs with higher efficiency and stability.

METHODS

Device fabrication

An ITO-patterned (15 mm × 2 mm) quartz substrate (20 mm × 3 mm) was ultrasonically cleaned with 2-propanol and acetone. A ZnO (electron transport layer, 40 nm) layer was prepared by spin-coating (1500 rpm, 15 s) a diluted solution of ZnO nanoparticles. PTzBT, ITIC, and $PC_{61}BM$ (purchased form Solenne BV) (1:0.2:2 w/w/w) dissolved in chlorobenzene solvent (approximately $5\,g\,L^{-1}$ concentration based on the PTzBT) was mixed at 100 °C for 30 min with a vibrational method. Then, the active layer was spin-coated (600 rpm, 20 s) on the ITO substrate in the nitrogen-filled glove box ($O_2 < 0.2$ ppm, $H_2O < 0.5$ ppm). The MoO_x (hole transport layer, 7.5 nm) and Ag (hole collecting electrode, 100 nm) layers were fabricated by a vacuum-deposition method below 4.0×10^{-5} Pa. The active area is 10 mm × 2.6 mm[8,10–12]. Thin films of PTzBT:ITIC:$PC_{61}BM$ (1:0.2:2 w/w/w) and PTzBT:$PC_{61}BM$ (1:2 w/w) were spin-coated (600 rpm, 20 s) on a quartz substrate (20 mm × 3 mm) with the same condition used for cells. Thin films and layered films of ZnO, ITIC, ZnO/$PC_{61}BM$, and ZnO/$PC_{71}BM$ were spin-coated on the quartz substrate with the same condition used for cells using spin-coating conditions for ZnO (1500 rpm, 15 s) and for ITIC, $PC_{61}BM$, and $PC_{71}BM$ (600 rpm, 20 s)[8,10–12]. MoO_x thin films (7.5 nm) were fabricated on the quartz substrate by the vacuum-deposition method with the same condition used for cells. The wiring details of a cell are schematized in Fig. 1d and Supplementary Fig. 6. All the samples were encapsulated in an ESR sample tube in the glove box. Other details are described in the references[10–12].

Device performance of PTzBT ternary solar cells

The device performance of the PTzBT cells is shown in Supplementary Fig. 4. The reason for the high ITIC response that extends to over 800 nm is an interference effect caused by the reflection of light at the metal electrode, which have been clarified by the optical measurements and simulations in the previous study[8]. Other details are described in the reference[8].

REFERENCES

1. Günes, S., Neugebauer, H. & Sariciftci, N. S. Conjugated polymer-based organic solar cells. Chem. Rev. 107, 1324–1338 (2007).
2. Clarke, T. M. & Durrant, J. R. Charge photogeneration in organic solar cells. Chem. Rev. 110, 6736–6767 (2010).
3. Søndergaard, R., Hösel, M., Angmo, D., Larsen-Olsen, T. T. & Krebs, F. C. Roll-to-roll fabrication of polymer solar cells. Mater. Today 15, 36–49 (2012).
4. Lin, Y. et al. An electron acceptor challenging fullerenes for efficient polymer solar cells. Adv. Mater. 27, 1170–1174 (2015).
5. Kim, T. et al. Morphology-dependent hole transfer under negligible HOMO difference in non-fullerene acceptor-based ternary polymer solar cells. ACS Appl. Mater. Interfaces 11, 7208–7215 (2019).
6. Ma, Y. et al. A minimal benzo[c][1,2,5]thiadiazole-based electron acceptor as a third component material for ternary polymer solar cells with efficiencies exceeding 16.0%. Mater. Horiz. 7, 117–124 (2020).
7. An, Q. et al. Alloy-like ternary polymer solar cells with over 17.2% efficiency. Sci. Bull. 65, 538–545 (2020).
8. Saito, M. et al. Significantly sensitized ternary blend polymer solar cells with a very small content of the narrow-band gap third component that utilizes optical interference. Macromolecules 53, 10623–10635 (2020).
9. Nagamori, T. & Marumoto, K. Direct observation of hole accumulation in polymer solar cells during device operation using light-induced electron spin resonance. Adv. Mater. 25, 2362–2367 (2013).
10. Kubodera, T. et al. Operando direct observation of charge accumulation and the correlation with performance deterioration in PTB7 polymer solar cells. ACS Appl. Mater. Interfaces 10, 26434–26442 (2018).
11. Rachmat, V. A. S. A., Kubodera, T., Son, D., Cho, Y. & Marumoto, K. Molecular oriented charge accumulation in high-efficiency polymer solar cells as revealed by operando spin analysis. ACS Appl. Mater. Interfaces 11, 31129–31138 (2019).

12. Xue, D., Kamiya, S., Saito, M., Osaka, I. & Marumoto, K. Direct evidence of less charge accumulation in highly durable polymer solar cells using operando electron spin resonance spectroscopy. *ACS Appl. Energy Mater.* **3**, 2028–2036 (2020).

13. Soon, Y. W. et al. Correlating triplet yield, singlet oxygen generation and photochemical stability in polymer/fullerene blend films. *Chem. Commun.* **49**, 1291–1293 (2013).

14. Clark, M. D., Jespersen, M. L., Patel, R. J. & Leever, B. J. Ultra-thin alumina layer encapsulation of bulk heterojunction organic photovoltaics for enhanced device lifetime. *Org. Electron.* **15**, 1–8 (2014).

15. Abdel-Fattah, T. M. et al. Stability study of low and high band gap polymer and air stability of PTB7:PC$_{71}$BM bulk heterojunction organic photovoltaic cells with encapsulation technique. *Synth. Met.* **209**, 348–354 (2015).

16. Marumoto, K., Kuroda, S., Takenobu, T. & Iwasa, Y. Spatial extent of wave functions of gate-induced hole carriers in pentacene field-effect devices as investigated by electron spin resonance. *Phys. Rev. Lett.* **97**, 256603 (2006).

17. Marumoto, K. et al. Microscopic mechanisms behind the high mobility in rubrene single-crystal transistors as revealed by field-induced electron spin resonance. *Phys. Rev. B* **83**, 075302 (2011).

18. Son, D., Kuwabara, T., Takahashi, K. & Marumoto, K. Direct observation of UV-induced charge accumulation in inverted-type polymer solar cells with a TiO$_x$ layer: Microscopic elucidation of the light-soaking phenomenon. *Appl. Phys. Lett.* **109**, 133301 (2016).

19. Sato, G. et al. Direct observation of radical states and the correlation with performance degradation in organic light-emitting diodes during device operation. *Phys. Status Solidi A* **215**, 1700731 (2018).

20. Biskup, T. et al. Ordering of PCDTBT revealed by time-resolved electron paramagnetic resonance spectroscopy of its triplet excitons. *Angew. Chem. Int. Ed.* **54**, 7707–7710 (2015).

21. Krinichnyi, V. I. & Yudanova, E. I. Influence of morphology of low-band-gap PCDTBT:PC$_{71}$BM composite on photoinduced charge transfer: LEPR spectroscopy study. *Synth. Met.* **210**, 148–155 (2015).

22. Tayebjee, M. J. Y. et al. Quintet multiexciton dynamics in singlet fission. *Nat. Phys.* **13**, 182–188 (2017).

23. Salvadori, E. et al. Ultra-fast spin-mixing in a diketopyrrolopyrrole monomer/fullerene blend charge transfer state. *J. Mater. Chem. A* **5**, 24335–24343 (2017).

24. Kobori, Y., Ako, T., Oyama, S., Tachikawa, T. & Marumoto, K. Transient electron spin polarization imaging of heterogeneous charge-separation geometries at bulk-heterojunction interfaces in organic solar cells. *J. Phys. Chem. C.* **123**, 13472–13481 (2019).

25. Yin, Z., Wei, J. & Zheng, Q. Interfacial materials for organic solar cells: Recent advances and perspectives. *Adv. Sci.* **3**, 1500362 (2016).

26. Nam, M. et al. Long-term efficient organic photovoltaics based on quaternary bulk heterojunctions. *Nat. Commun.* **8**, 14068 (2017).

27. Schmidt-Mende, L. & MacManus-Driscoll, J. L. ZnO - nanostructures, defects, and devices. *Mater. Today* **10**, 40–48 (2007).

28. Xue, D., Kamiya, S., Saito, M., Osaka, I. & Marumoto, K. Analyses of PTzNTz polymer solar cells using ESR spectroscopy. *J. Photopolym. Sci. Technol.* **33**, 97–102 (2020).

29. Tamai, Y. et al. Light-induced degradation mechanism in Poly(3-hexylthiophene)/Fullerene blend solar cells. *Adv. Energy Mater.* **6**, 1600171 (2016).

30. Osaka, I., Saito, M., Koganezawa, T. & Takimiya, K. Thiophene-thiazolothiazole copolymers: Significant impact of side chain composition on backbone orientation and solar cell performances. *Adv. Mater.* **26**, 331–338 (2014).

31. Mardis, K. L., Webb, J. N., Holloway, T., Niklas, J. & Poluektov, O. G. Electronic structure of fullerene acceptors in organic bulk-heterojunctions: A combined EPR and DFT study. *J. Phys. Chem. Lett.* **6**, 4730–4735 (2015).

32. Zhang, M. et al. Defect-related multicolour emissions in ZnO smoke: from violet, over green to yellow. *Nanoscale* **11**, 5102–5115 (2019).

33. Xue, D., Saito, M., Osaka, I. & Marumoto, K. Analyses of charge accumulation of PTzBT ternary polymer solar cells using ESR spectroscopy. *J. Photopolym. Sci. Technol.* **34**, 351–356 (2021).

34. Cheyns, D. et al. Analytical model for the open-circuit voltage and its associated resistance in organic planar heterojunction solar cells. *Phys. Rev. B* **77**, 165332 (2008).

AUTHOR CONTRIBUTIONS

D.X. and K.M. planned the study. M.S. and I.O. synthesized PTzBT and ITIC molecules and ZnO precursor. D.X. and K.M. fabricated and measured the cells, and analyzed the data. D.X. and K.M. wrote the paper. All authors discussed the results and reviewed the manuscript.

COMPETING INTERESTS

The authors declare no competing interests.

ADDITIONAL INFORMATION

Supplementary information The online version contains supplementary material available at https://doi.org/10.1038/s41528-022-00153-z.

Correspondence and requests for materials should be addressed to Kazuhiro Marumoto.

Reprints and permission information is available at http://www.nature.com/reprints

Publisher's note Springer Nature remains neutral with regard to jurisdictional claims in published maps and institutional affiliations.